Available online at www.sciencedirect.com
SCIENCE DIRECT
ELSEVIER
Journal of the European Ceramic Society 26 (2006) 2327–2336
ECERS
www.elsevier.com/locate/jeurceramsoc

Effect of doping method on microstructural and defect profile of Sb–$BaTiO_3$

E. Brzozowski [a], A.C. Caballero [b], M. Villegas [b], M.S. Castro [a,*], J.F. Fernandez [b]

[a] *Institute of Materials Science and Technology (INTEMA), CONICET, Universidad Nacional de Mar del Plata, Av. Juan B. Justo 4302, B7608FDQ Mar del Plata, Argentina*
[b] *Ceramics for Smart Systems Group, Electroceramic Department, Instituto de Cerámica y Vidrio, CSIC, c/Kelsen s/n, 28049 Madrid, Spain*

Received 22 December 2004; received in revised form 4 April 2005; accepted 14 April 2005
Available online 13 June 2005

Abstract

Electrical properties in $BaTiO_3$ based ceramics are strongly dependent on composition and microstructural development. In this work, we studied the effect of the particle coating as doping method on microstructure and electrical properties of Sb-doped $BaTiO_3$. The advanced doping method involved surface-coated $BaTiO_3$ particles with a thin film of a metal-organic precursor solution. Results were compared with the performance obtained on conventional doping method. The particle coating as doping method led to an effective grain growth inhibition as well as significant microstructure improvement.

The incorporation of dopant into the perovskite lattice is influenced by the doping method. Results suggested that Sb acted as donor dopant on A or/and B sites, and also as acceptor on B sites, modifying the grain boundaries structure characteristics. Dopant incorporation method affected the defect structure, and therefore, the donor dopant concentration for the semiconductor insulator transition in $BaTiO_3$ ceramics.

Keywords: Grain growth; Defects; Microstructure-final; Electrical conductivity; $BaTiO_3$ and titanates

1. Introduction

Barium titanate ceramic is a well-known ferroelectric ceramic that has been of practical importance for about 50 years because of its excellent dielectric properties. Donor doped $BaTiO_3$ ceramics introduced n-type semiconductor characteristic and exhibit a positive temperature coefficient of resistivity (PTCR). Intergranular barrier layers at the grain boundaries govern the electrical properties in $BaTiO_3$ based ceramics.[1] Additionally, additive incorporation modifies the ionic defect structure and the charge compensation mechanisms. On this matter, it was observed that after addition of 0.3% at. Nb_2O_5, La_2O_3, Sb_2O_3 or MnO_2 among others, insulating $BaTiO_3$ becomes semiconductor.[1] Further oxide concentration reverts the semiconductor behaviour to insulator.[2–5] In addition to the electrical transition at 0.3% at. of dopant, refinement of the grains on sintering is usually reported.[6–8] Studies suggest that changes in electrical behaviour and grain growth inhibition phenomena are ruled by a change in the charge compensation mechanism on dopant incorporation.[9] The electrical features of semiconducting $BaTiO_3$ ceramics depend crucially on the microstructure and characteristics of grain boundaries which were influenced by the composition and processing.

The microstructure of $BaTiO_3$ ceramics is significantly influenced by the Ba/Ti ratio. For stoichiometric samples, fine-grain and porous microstructures are observed. For the Ba-rich samples, small-grain microstructures are maintained but density is high, resulting from modification of defect chemistry by excess Ba^{2+} ions. In Ti-rich, liquid-phase sintering occurs when the sintering temperature is greater than the corresponding eutectic temperature, and large-grain microstructure is obtained. The semiconductor behaviour is closely related to the microstructure. High electrical resistivity and poor PTCR effect are generally observed for

* Corresponding author.
E-mail address: mcastro@fi.mdp.edu.ar (M.S. Castro).

0955-2219/$ – see front matter © 2005 Elsevier Ltd. All rights reserved.
doi:10.1016/j.jeurceramsoc.2005.04.017

the fine-grained materials.[10] Small room temperature resistivity and good PTCR characteristics are, on the contrary, generally found for the large-grained materials. However, good PTCR behaviour in fine-grained ceramics can also be achieved by adequate cooling because of the barium vacancies compensation.[10] The liquid sintering promotes grain growth and ensured dopant diffusion into perovskite lattice. Recently, boron based sintering aids are effective in the liquid-phase sintering of Nb-semiconducting $BaTiO_3$ ceramics because the sintering aids do not diffuse into the grains during sintering.[11]

In the last years, it has been recognised the importance of preparation methods on the performance of a given additive.[12–15] Nevertheless, the influence of ceramic processing on defect structure at the grain boundaries of $BaTiO_3$ ceramics, and hence, on electrical properties is at present not fully understood.

In this paper, we studied the effect of an advanced doping method (particles coating) on the performance of a given additive. On the basis of microstructural development and defect profile results coupled with electrical properties, the advanced doping method was compared with the traditionally oxide doping method used in $BaTiO_3$ ceramics.

2. Experimental

Base materials were prepared from technically pure $BaTiO_3$ powder (Elmic BT100, Rhone Poulenc, particle size 0.84 μm, Ba/Ti 1.000, purity 99.9%, main impurity Sr <0.05%). A first set of samples was prepared with $BaTiO_3$ particles doped with 0.05, 0.15, 0.30 or 0.60 mol% of Sb_2O_3 (Aldrich, 99.99%, mean particle size 2 μm) via a conventional mixed oxide method (named as oxide method). A second set of samples was prepared with $BaTiO_3$ powder doped with 0.05, 0.15, 0.30 or 0.60 mol% equivalent to Sb_2O_3 via a particles coating method[16] (named as coating method). In the coating method, dopant was incorporated by dropping a $Sb(O(CH_3)_3(CH_3)_3)_3$ (antimony butoxide, Aldrich, density 1.225 g/cm^3) solution in an alcoholic suspension of $BaTiO_3$ particles. In both routes, raw materials were mixed in the alcoholic medium for 5 min with a high-speed turbine. Dried powders were isostatically pressed at 200 MPa and sintered in air at temperatures ranged from 1300 to 1400 °C, with a heating/cooling rate of 3 °C/min and sintering time of 2 h.

Density measurements were carried out in water employing a Sartorious kit based in the Archimedes method. Dilatometric analyses (Adamel Lhomargy DI24) were performed on isostatically pressed bars at a heating rate of 3 °C/min. Scanning electron microscopy (SEM) (Philips 505) evaluated microstructures on fractured, polished and thermally etched samples of $BaTiO_3$-doped ceramics. Energy-dispersive spectroscopy (EDS) (EDX DX Prime 10) coupled to the scanning electron microscopy determined phase composition. X-ray analyses were conducted to determine second phases and lattice distortion in crushed $BaTiO_3$ ceramics. Tetragonality parameter (c/a) was calculated from the reflections of (2 0 0) and (0 0 2) planes scanned between 44 and 47° at 0.125°/min, using a Philips PW 1050/25 equipment with Cu Kα radiation and Ni filter at 40 kV and 20 mA.

To characterise the paramagnetic species in the crushed samples at room temperature, a Bruker ER-200D (Band X) EPR spectroscope with a gain of 2×10^4, a power of 5 dB and modulation amplitude of 6.3 Gpp was used. The EPR signal intensities were labelled as double integrated intensities (DII) calculated from the empirical relation reported by Murugaraj et al.[17]:

$$\mathrm{DII} = \frac{[(\text{signal height})(\text{signal width})]}{[(\text{gain})(\text{sample mass})(\text{modulation amplitude})\ (\text{power})^{1/2}]} \quad (1)$$

Finally, resistivity was measured on silver-electroded discs at room temperature using an electrometer (Keithley 614) applying 0.01 V.

3. Results

As follow from dilatometric measurements (Fig. 1), incorporation of dopant by coating method promoted earlier densification. In addition, maximum shrinkage took place below 1250 °C (Fig. 1A and B). In oxide-mixed materials, sintering behaviour varied remarkably in dependence on dopant content, $BaTiO_3$ doped with 0.05 mol% of Sb_2O_3 started at higher temperatures than 1250 °C and progressed slower (Fig. 1C and D), meanwhile doping with 0.60 mol% of Sb_2O_3 maximum shrinkage took place below 1250 °C. The oxide method led to lower sintering rates than the coating method.

In those materials doped through the coating method, fully densified materials (96–98%) were attained with minimum dopant concentrations (0.05–0.15 mol% of Sb_2O_3) and sintering temperatures (1300 °C) below the eutectic temperature (1320 °C) (Figs. 2–5). As follow from Fig. 6, effective grain growth inhibition took place on doping through the coating method.

In oxide method, the ceramics with 0.05–0.60 mol% of Sb_2O_3 sintered at 1300 °C, showed abnormal grain growth (Fig. 7). In this case, characteristic large grains with intragranular porosity embedded in a fine-grained matrix of $BaTiO_3$ were observed. High-density values could be only reached on doping with >0.15 mol% Sb_2O_3 and sintering at >1350 °C (Figs. 2 and 3). In fact, oxide method for doped ceramics reaches a more uniform microstructure when sintered at 1350 °C, indicating a homogenisation process by diffusion (Fig. 8).

In coating and oxide methods, ceramics with 0.30 or 0.60% Sb_2O_3 developed second phases on sintering above 1320 °C. On sintering at 1375–1400 °C, second phases formation was already detected for 0.15 mol% of Sb_2O_3. Morphology and distribution of second phases varied in dependence on doping method. In oxide method,

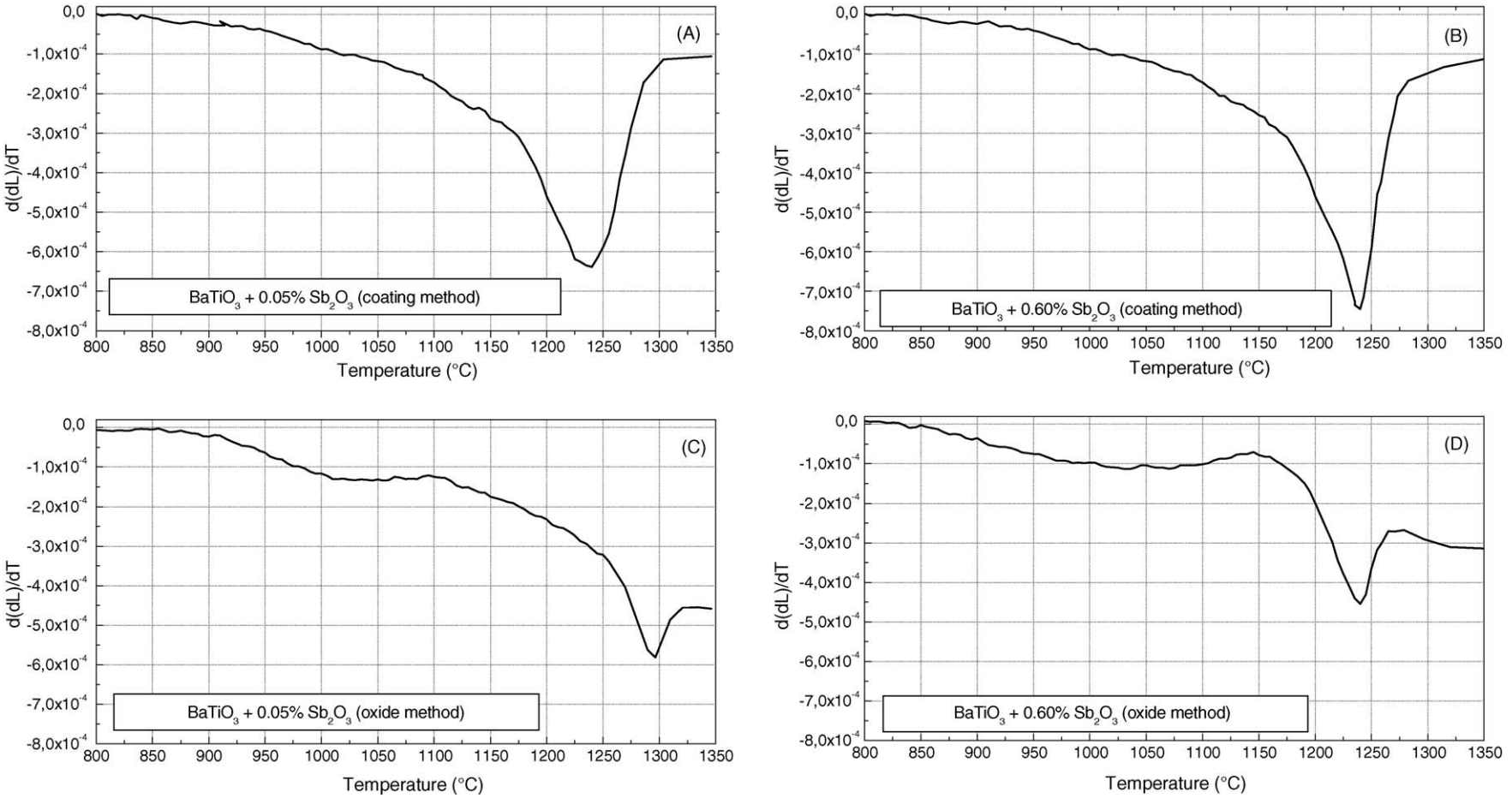

Fig. 1. Sintering velocity in a dilatometer experiment of samples with 0.05 and 0.60 mol% equivalent Sb_2O_3.

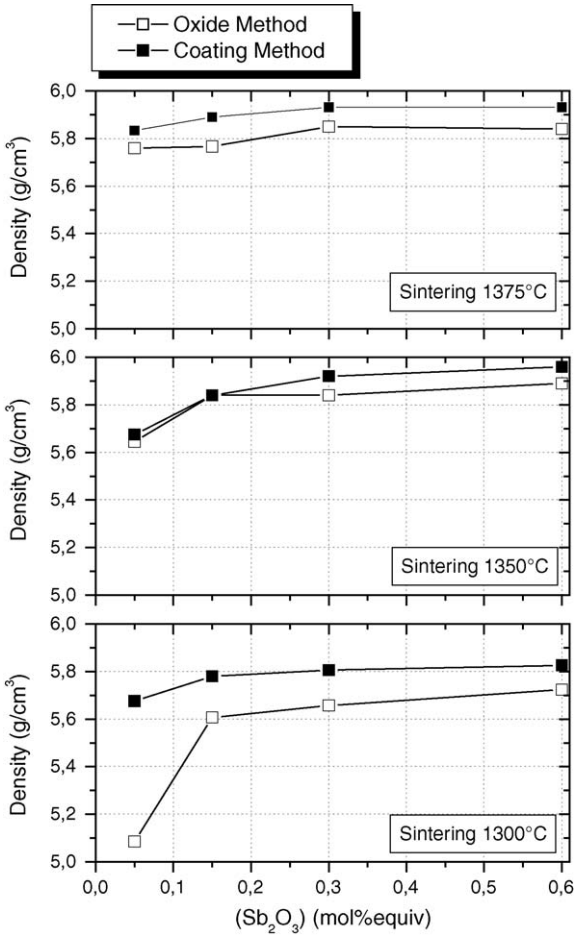

Fig. 2. Density vs. dopant concentration for samples sintered at 1300, 1350 and 1375 °C.

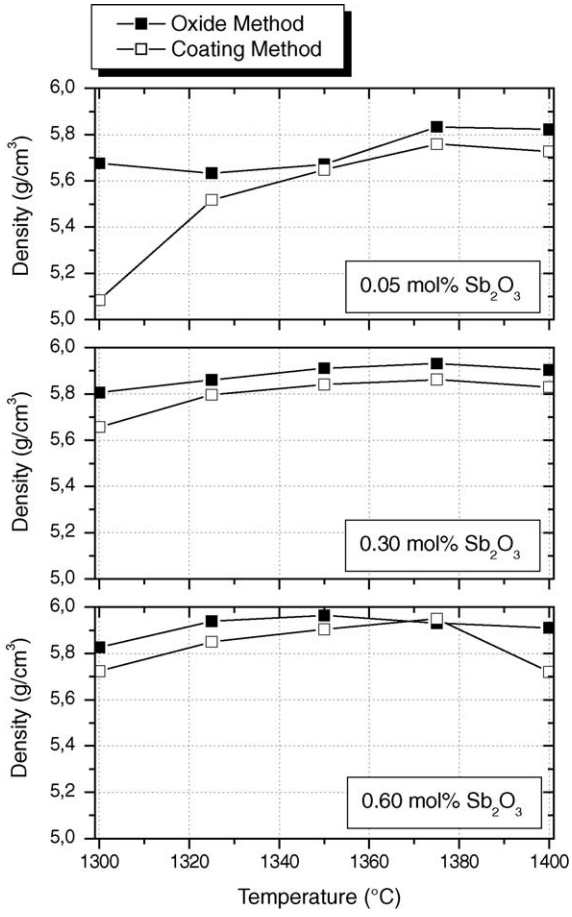

Fig. 3. Density vs. sintering temperature for samples doped with 0.05, 0.30 and 0.60 mol% of equivalent Sb_2O_3.

needle-shaped second phases appeared on fine-grain regions (Fig. 9A). Semi quantitative EDS analyses performed on randomly chosen needles showed a fluctuation of Ti/Ba ratio respect to the nominal ratio for the given $BaTiO_3$ composition (Table 1). In the coating method, a second phase with similar morphology was also detected (Fig. 9B). In addition, a glassy phase covering fine-grained is shown for sintering temperatures higher than 1320 °C. Table 1 shows the Ba/Ti scattering data collected by EDS analyses for samples sintered at 1350 °C.

Dopant incorporation into the perovskite lattice was also reflected on the tetragonal distortion. XRD profiles showed an evolution from a tetragonal structure split in two peaks (Fig. 10) to a pseudocubic structure with a single peak merging at $2\theta = 46.5$ for the highest dopant concentration (0.60 mol% Sb_2O_3). Pseudocubic stabilisation was more noticeable in ceramics doped through the coating method, as followed from the significant broadening of their diffraction peaks. Fig. 10 also shows the evolution of lattice parameters (c/a) with dopant concentration on sintering at 1300 or 1350 °C. Lattice parameters for oxide method doped materials showed a maximum for the 0.05% Sb_2O_3 concentration and decreased on further dopant incorporation. In materials doped by the coating method, c/a decreased continuously on dopant addition (Fig. 10).

Table 1
Ti/Ba elemental ratio by EDX in Sb-doped $BaTiO_3$ sintered at 1350 °C

Sb_2O_3 (mol%)	Ti/Ba (bulk)	Ti/Ba (second phase)
Oxide method		
0.30	1.10	0.77
0.60	1.10	2.00
Coating method		
0.30	0.91	2.10
0.60	1.13	2.00

The EPR analyses revealed two singlets with variable intensity at $g = 2.003$ and 1.973 and a weak signal at $g = 1.932$. A recent article on $BaTiO_3$ defects associated EPR singlets with $g = 2.003$ and 1.973 to intrinsic point defects, V_{Ti} (probably V'_{Ti} or V'''_{Ti}) and V'_{Ba}, respectively.[18] Koodiazhnyi and Petric reported an increment of EPR singlet intensities at the Curie temperature coupled with a PTCR effect.[18] Several authors[17,18] observed the signal at $g = 1.932$ in n-semiconducting $BaTiO_3$ ceramics, which became negligible on further oxidation. Based on the literature, the signal with $g = 1.932$ is assigned to Ti^{3+} and its related to complex

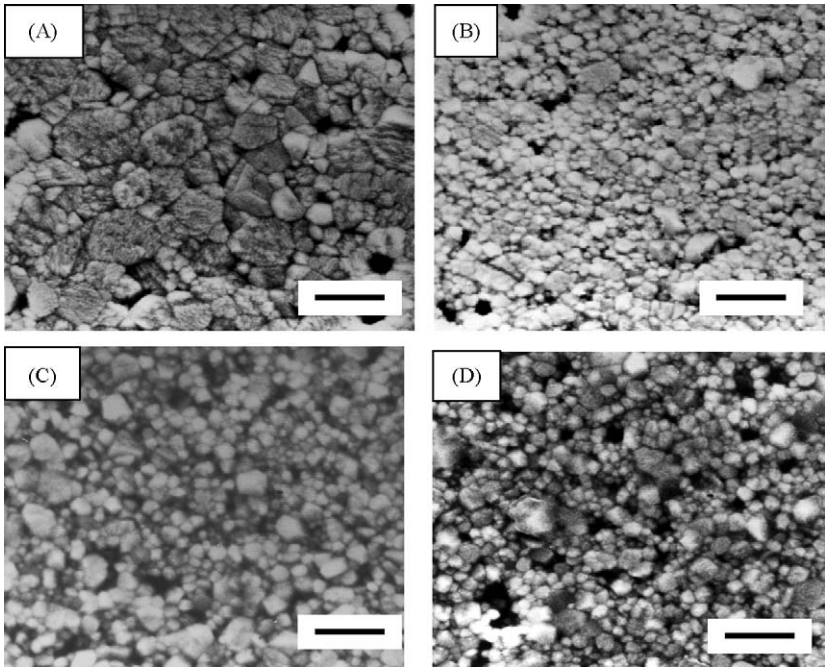

Fig. 4. SEM micrographs for coating method based ceramics sintered at 1300 °C. (A) 0.05 mol%; (B) 0.15 mol%; (C) 0.30 mol%; and (D) 0.60 mol% equivalent Sb_2O_3. Bar = 10 μm.

Ti^{3+}–Vo, as it was proposed by Koodiazhnyi and Petric[18] and Scharfschwerdt et al.[19] Besides the mentioned singlet, a sextet lying at $g = 1.974$ attributed to Mn^{2+} impurity in $BaTiO_3$ was observed.[17–20]

Evolution of EPR signals for ceramic from both the coating method and the oxide method sintered at 1350 °C is detailed in Fig. 11. Ionic defects detected for unmodified $BaTiO_3$ were attributed to inherent ionic vacancies compensating for natural impurities.

In oxide method samples, titanium vacancies concentration remained lower than barium vacancies concentration in the whole compositional range. However, at 0.30 mol%

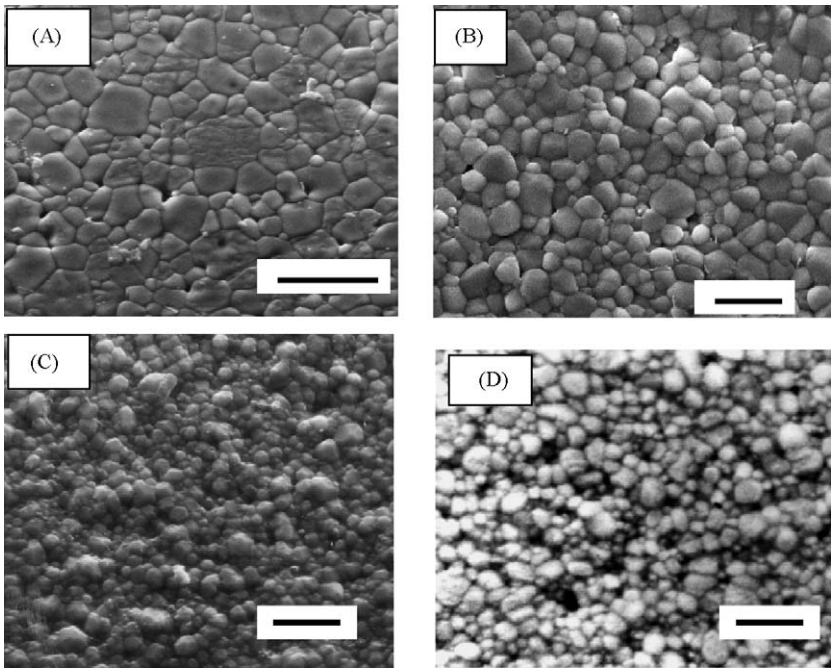

Fig. 5. SEM micrographs for coating method based ceramics sintered at 1350 °C. (A) 0.05 mol%; (B) 0.15 mol%; (C) 0.30 mol%; and (D) 0.60 mol% equivalent Sb_2O_3. Bar = 10 μm.

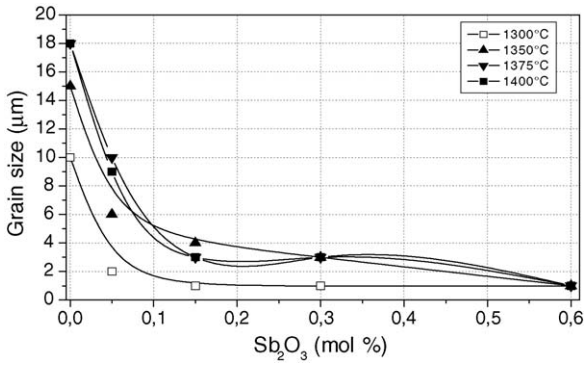

Fig. 6. Grain size vs. dopant concentration for coating method based ceramics sintered between 1300 and 1400 °C.

of Sb_2O_3, concentration of titanium vacancies increased slightly. Maximum barium vacancies concentration in oxide method ceramics was achieved at 0.05 mol% of Sb_2O_3. After this threshold, barium vacancies concentration decreased and remained nearly unaffected on further dopant additions. The weak singlet with $g = 1.932$ attributed to Ti^{3+}–Vo was indeed observed for unmodified and oxide method ceramics doped with 0.05–0.60 mol% of Sb_2O_3. This signal became negligible at high doping levels, being overlapped with the Mn^{2+} sextet.

Materials doped through the coating method showed a different trend in dependence on the dopant concentration range. Titanium vacancies concentration remained lower than barium vacancy concentration in the small dopant incorporation range up to 0.15 mol% of Sb_2O_3. In this range, barium vacancies concentration increased. However, a drastic increase in titanium vacancies concentration was observed after 0.15 mol% Sb_2O_3. In addition, a slight decrease in barium vacancies content was observed. The Ti^{3+}–Vo signal with $g = 1.932$ was observed on coated systems in the small concentration range between 0.05 and 0.15% Sb_2O_3, but it was absent on further dopant incorporation. In addition, intensity of Mn^{2+} sextet was significantly high on doping with 0.30 or 0.60 mol% of Sb_2O_3.

Fig. 12 details the electrical parameters measured at room temperature for samples sintered at 1350 °C. Room temperature resistivity for the conventionally prepared materials decreased on doping up to 0.30 mol% Sb_2O_3 and increased on further dopant addition. Materials doped by the coating method attained their minimum resistivity at 0.05 mol% Sb_2O_3.

4. Discussion

When doping of $BaTiO_3$ particles was carried out by the coating method, effective dopant distribution was achieved. Because the organic precursor coated the $BaTiO_3$ particles, short diffusion pathways of dopant toward the barium titanate nuclei were established. Dopant reacted at low temperatures and early densification was promoted (Fig. 1). As an evidence of the high uniform dopant distribution, the grain growth inhibition is very effective. The abnormal grain growth typical of low dopant concentration is avoided. Thus, fine-grained and homogeneous microstructures were achieved in a wide range of temperatures (Figs. 4–6). Above the 1320 °C threshold, titanium segregation in highly doped microstructures led to a glassy phase covering fine-grains.

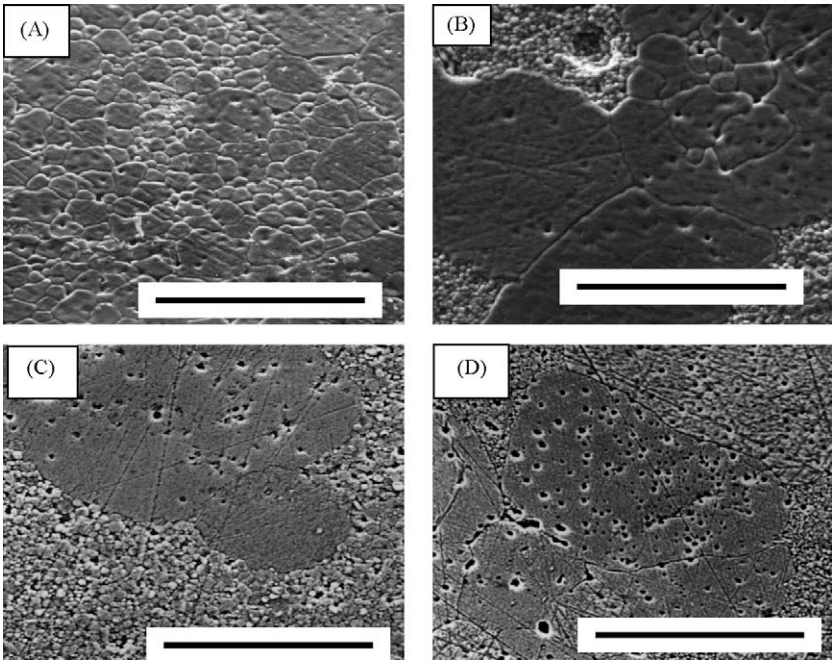

Fig. 7. SEM micrographs for oxide method based ceramics sintered at 1300 °C. (A) 0.05 mol%; (B) 0.15 mol%; (C) 0.30 mol%; and (D) 0.60 mol% Sb_2O_3. Bar = 100 μm.

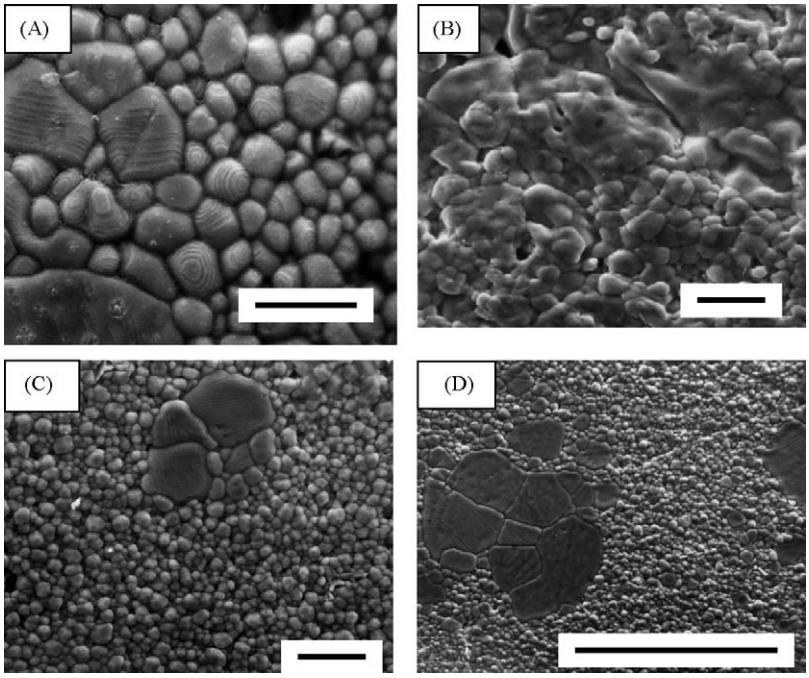

Fig. 8. SEM micrographs for oxide method based ceramics sintered at 1350 °C. (A) 0.05 mol%; (B) 0.15 mol%; (C) 0.30 mol%; and (D) 0.60 mol% Sb_2O_3. Bar = 10 μm.

Non-uniform dopant distribution through oxide method failed to control the development of grains and pointed to abnormal grain growth (Figs. 7 and 8). Microstructures advanced in different fashion depending on local dopant concentration. Enriched Sb regions led to grain growth inhibition, Ti segregation and second phase formation. Regions with low dopant incorporation led to intra-grain porosity, abnormal grains and relatively low densification level. Microstructures became homogeneous and fine-grained as the nominal Sb_2O_3 oxide concentration approached 0.60 mol% and sintering temperatures higher than 1350 °C, due to more effective dopant incorporation in the $BaTiO_3$ particles. The two different second phases with Ba-rich or Ti-rich compositions detected in oxide-highly doped materials indicated a competence of two different Sb incorporation modes in dependence on local dopant concentration (Table 1).

XRD signals were related to Sb incorporation on A or B sites of the perovskite lattice, grain refinement and ferroelectric domain walls motion. The well-defined tetragonal peaks from the 0.05 mol% Sb_2O_3 oxide method doped materials revealed domains formation in coarse $BaTiO_3$ grains. As far as dopant was incorporated into the $BaTiO_3$, a significant XRD distortion was observed (Fig. 10). Substitution of Sb^{3+} (ionic radius 0.76 Å) for Ba^{2+} (ionic radius 1.34 Å) or Sb^{5+} (ionic radius 0.62 Å) for Ti^{4+} (ionic radius 0.68 Å) decreased the *c*/*a* ratio. Incorporation of Sb^{3+} on Ti^{4+} sites increased *c*/*a* ratio (Fig. 10).

Dopant incorporation in $BaTiO_3$ sintered at 1350 °C was well depicted by the room temperature electrical measurements in combination with EPR results. Unmodified $BaTiO_3$ showed inherent high resistivity $>10^{10}$ Ω cm that remark the absence of impurities in the raw material particles. Conduc-

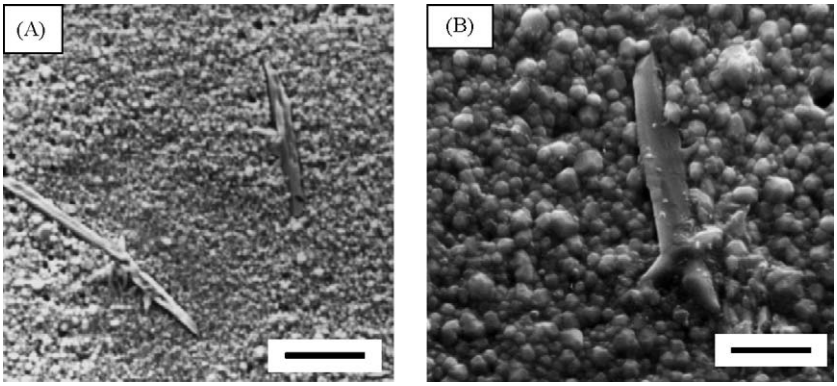

Fig. 9. Second phases in (A) oxide method and (B) coating method based ceramics sintered at 1350 °C.

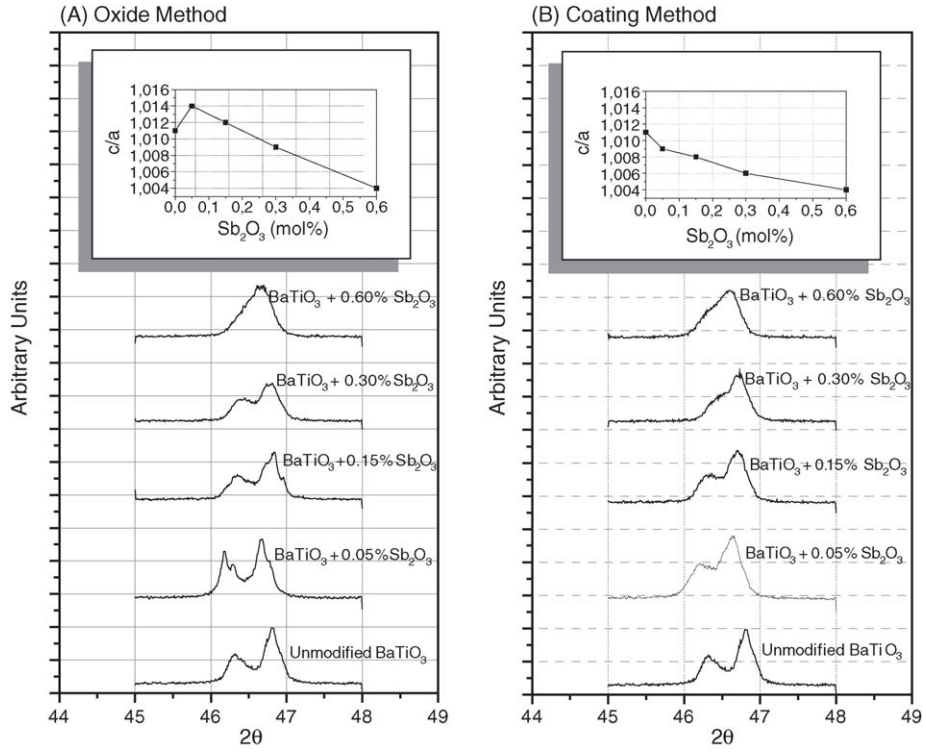

Fig. 10. (Bottom) XRD signals for (A) oxide method and (B) coating method based ceramics sintered at 1350 °C. In the insert, the Tetragonality parameters (*c*/*a*) vs. dopant concentration was shown for both methods.

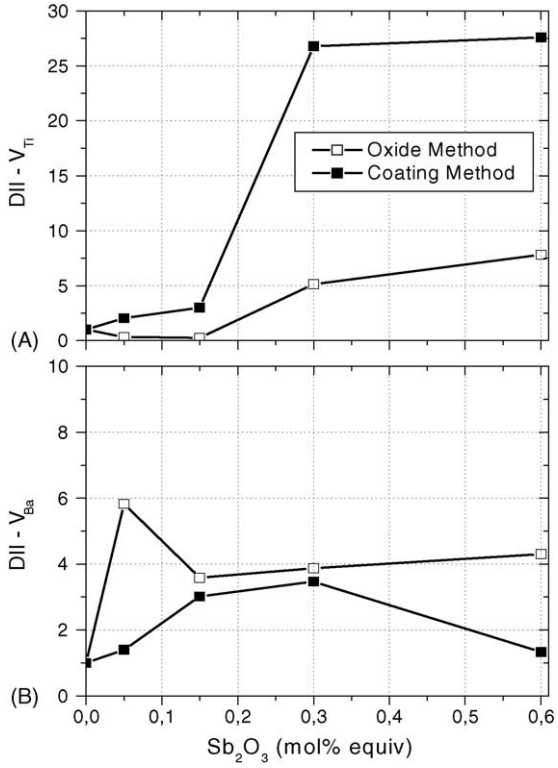

Fig. 11. Double integrated EPR intensity (DII) vs. dopant concentration for (A) titanium vacancies and (B) barium vacancies.

tivity increased with dopant concentration and reached its maximum value at 0.05 mol% Sb_2O_3 (Fig. 12) for the coating method ceramics. In this case, an electronic compensation mechanism predominated:

$$Sb_2O_3 + 2Ba_{Ba} \rightarrow 2Sb_{Ba}^{\bullet} + 2e' + \tfrac{1}{2}O_2 + 2BaO \quad (2)$$

where Sb^{3+} acted as donor on replacing Ba^{2+} ions.

Stabilisation of Sb^{5+} must not be neglected:

$$Sb_2O_5 + 2Ti_{Ti} \rightarrow 2Sb_{Ti}^{\bullet} + 2e' + \tfrac{1}{2}O_2 + 2TiO_2 \quad (3)$$

which also contributed to increase the conductivity. Substitution of Sb^{3+} and/or Sb^{5+} for Ba^{2+} or Ti^{4+} ions, respectively,

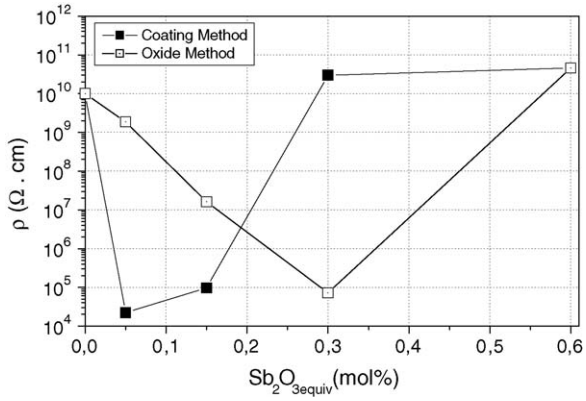

Fig. 12. Resistivity vs. dopant concentration for ceramics sintered at 1350 °C.

in 0.05% Sb_2O_3 coating method decreased *c*/*a* and increased conductivity by Eqs. (2) and (3).

The variation of barium vacancy concentration detected in the samples on further dopant addition obeyed to:

$$Sb_2O_3 + 3Ba_{Ba} \rightarrow 2Sb_{Ba}^{\bullet} + V_{Ba}'' + 3BaO \quad (4)$$

$$Sb_2O_5 + 2Ti_{Ti} + Ba_{Ba} \rightarrow 2Sb_{Ti}^{\bullet} + V_{Ba}'' + TiO_2 + BaTiO_3 \quad (5)$$

According to Schmelz,[21] the Sb ions occupy the Ti sites (Eqs. (3) and (5)) in the $BaTiO_3$ lattice and only in the case of an excess of Ti, it would also go on Ba sites (Eqs. (2) and (4)).

Also, for high doping level, the titanium vacancy formation must be considered:

$$2Sb_2O_3 + Ti_{Ti} + 4Ba_{Ba} \rightarrow 4Sb_{Ba}^{\bullet} + V_{Ti}'''' + 3BaO + BaTiO_3 \quad (6)$$

$$2Sb_2O_5 + 5Ti_{Ti} \rightarrow 4Sb_{Ti}^{\bullet} + V_{Ti}'''' + 5TiO_2 \quad (7)$$

Eqs. (4)–(7) did not provide free carriers and the material reverted to high-resistive behaviour.

In the oxide method materials, conductivity and defect structure were sensitive to non-uniform dopant distribution. The Ti^{3+}–V_O–Ti^{4+} defect centres in conventionally doped materials obeyed to the substitution of Sb^{3+} (ionic radius 0.76 Å) for Ti^{4+} (0.68 Å) on dopant-enriched zones:

$$Sb_2O_3 + 2Ti_{Ti} + O_o \rightarrow 2Sb_{Ti}' + V_O^{\bullet\bullet} + 2TiO_2 \quad (8)$$

where Sb^{3+} acted as acceptor on Ti^{4+} sites.

Incorporation of Sb^{3+} on B sites (Eq. (8)) expanded the $BaTiO_3$ lattice and enlarged the *c*/*a* ratio in 0.05–0.15% of Sb_2O_3 oxide method materials (Fig. 10). Dopant concentration range for maximum conductivity in conventional systems was reached at 0.30 mol% Sb_2O_3 that it is in well agreement with literature results.[1] Maximum conductivity is due to more uniform and complete incorporation of dopant through Eqs. (2) and (3) with the free carriers increasing and *c*/*a* tetragonality decreasing. Further dopant concentration favoured titanium vacancies and barium vacancies regimes and the material reverted to insulating features. In addition, significant Ti and Ba segregation occurring in the intergranular phase contributed to increase the resistivity. On the other hand, maximum conductivity in coating method was reached with 0.05 mol% of Sb_2O_3. This threshold is significatively lower than previously observed and could be clearly associated with the high dopant distribution. Further dopant addition increases titanium vacancies and the sample resistivity. According to the experimental results, dopant introduction by the coating method increases the dopant effectiveness, which allows the amount of dopant to be reduced.[12,22–24]

It is generally accepted that the critical doping level of 0.3 mol% is independent of the kind of additive, and it does not even depend on whether the additive atoms are placed in the A sites or in the B sites.[1] However, from the experimental results, the better additive distribution favours its incorporation to the $BaTiO_3$ lattice and the critical doping level diminution.

5. Conclusions

High homogeneity and fine-grained materials were successfully achieved on coating $BaTiO_3$ particles with an organic source of dopant. Compared with conventional doping, the coating method limited the natural trend for the abnormal grain growth and allowed to control microstructures at lower sintering temperatures and lower dopant contents.

The actual donor concentration was a sensitive function of the doping method employed. It led to different donor or acceptor incorporation modes in Sb-doped $BaTiO_3$ ceramics. In consequence, the critical donor concentration for the semiconductor–insulator transition in $BaTiO_3$ ceramics was remarkably shifted.

Acknowledgements

The authors express their thanks to the Programa CYTED (Project PI-VIII.13 PROALERTA), CONICET and Universidad Nacional de Mar del Plata (Argentina), and CICYT (Spain) (Project MAT2004-04843-C02-01) for their financial support.

References

1. Hozer, L., *Semiconductor Ceramics—Grain Boundary Effects*. PWN Polish Scientific Publishers, Warsaw, Poland, 1994, pp. 109–143.
2. Jonker, H., Some aspects of semi-conducting barium titanate. *Solid State Electron.*, 1964, **7**, 895–903.
3. Drofenik, M., Origin of the grain growth anomaly in donor-doped barium titanate. *J. Am. Ceram. Soc.*, 1993, **76**, 123–128.
4. Zajc, I. and Drofenik, M., Semiconducting $BaTiO_3$ ceramic prepared by low temperature liquid sintering. *J. Mater. Res.*, 1998, **13**, 660–664.
5. Li, Z. C. and Bergman, B., Electrical properties and ageing characteristics of $BaTiO_3$ ceramics doped by single dopants. *J. Eur. Ceram. Soc.*, 2005, **25**, 441–445.
6. Chan, H., Harmer, M. and Smyth, D., Compensating defects in higly donor-doped $BaTiO_3$. *J. Am. Ceram. Soc.*, 1986, **69**, 507–510.
7. Chiou, B.-S. and Warng, I.-H., Effect of MgO addition on the electrical transport properties of highly Sb-doped $BaTiO_3$ ceramics. *J. Mater. Sci.: Mater. Electron.*, 1998, **9**, 145–150.
8. Viviani, M., Buscaglia, M. T., Buscaglia, V., Mitoseriu, L., Testino, A., Nanni, P. *et al.*, Analysis of conductivity and PTCR effect in Er-doped $BaTiO_3$ ceramics. *J. Eur. Ceram. Soc.*, 2004, **24**, 1221–1225.
9. Brzozowski, E. and Castro, M. S., Grain growth control in Nb-doped $BaTiO_3$. *J. Mater. Process. Tech.*, in press.
10. Lin, T. F. and Hu, C. T., Influence of stoichiometry on the microstructure and positive temperature coefficient of resistivity of semiconducting barium titanate ceramics. *J. Am. Ceram. Soc.*, 1998, **73**(3), 531–536.
11. Wang, X., Chan, H. L. W. and Choy, C., Positive temperature coefficient of resistivity effect in niobium-doped barium titanate ceram-

ics obtained at low temperature. *J. Eur. Ceram. Soc.*, 2004, **24**, 1227–1231.
12. Fernández, J. F., Caballero, A. C., Durán, P. and Moure, C., Improving sintering behaviour of $BaTiO_3$ by small doping additions. *J. Mater. Sci.*, 1996, **31**, 975–981.
13. Qi, J., Li, L., Li, W., Wang, Y. and Gui, Z., The influence of doping style on the grain growth of $BaTiO_3$ ceramics. *Mater. Sci. Eng. B*, 2003, **99**, 214–216.
14. Stojanovic, B. D., Foschini, C. R., Zaghete, M. A., Veira, F. O. S., Peron, K. A., Cilense, M. *et al.*, Size effect on structure and dielectric properties of Nb-doped barium titanate. *J. Mater. Process. Tech.*, 2003, **143–144**, 802–806.
15. Park, M.-B. and Cho, N.-H., Chemical and structural features of the grain boundaries in semiconducting $BaTiO_3$ ceramics prepared from surface-coated powders. *Solid State Ionics*, 2002, **154–155**, 407–412.
16. Villegas, M., Jardiel, T., Caballero, A. C. and Fernández, J. F., Electrical properties of bismuth titanate based ceramics with secondary phases. *J. Electroceram.*, 2004, **13**, 534–548.
17. Murugaraj, P., Kutty, T. R. N. and Subba Rao, M., Diffuse phase transformations in neodymium-doped $BaTiO_3$ ceramics. *J. Mater. Sci.*, 1986, **21**, 3521–3527.
18. Kolodiazhnyi, T. and Petric, A., Analysis of point defects in polycrystalline $BaTiO_3$ by electron paramagnetic resonance. *J. Phys. Chem. Solids*, 2003, **64**, 953–966.
19. Scharfschwerdt, R., Mazur, A., Schimer, O. F., Hesse, H. and Mendricks, S., Oxygen vacancies in $BaTiO_3$. *Phys. Rev. B*, 1996, **54**, 15284–15290.
20. Jida, S. and Mike, T., Electron paramagnetic resonance of Nb-doped $BaTiO_3$ ceramics with positive temperature coefficient of resistivity. *J. Appl. Phys.*, 1995, **80**, 5234–5239.
21. Schmelz, H., Incorporation of antimony into the barium titanate lattice. *Phys. Stat. Sol.*, 1969, **31**, 121–128.
22. Caballero, A. C., Fernández, J. F., Villegas, M., Moure, C. and Durán, P., Intermediate phase development in phosphorous-doped barium titanate. *J. Am. Ceram. Soc.*, 2000, **83**, 1499–1505.
23. Hatano, T., Yamaguchi, T., Sakamoto, W., Yogo, T., Kikuta, K., Yoshida, H. *et al.*, Synthesis and characterization of $BaTiO_3$-coated Ni particles. *J. Eur. Ceram. Soc.*, 2004, **24**, 507–510.
24. Park, M.-B., Kim, C.-D., Lee, S.-K. and Cho, N.-H., Phase transition and dielectric characteristics of nano-grained $BaTiO_3$ ceramics synthesized from surface-coated nano-powders. *Appl. Surf. Sci.*, 2002, **190**, 416–421.